Printing in three dimensions with graphene

Esther García-Tuñon, Suelen Barg, Jaime Franco, Robert Bell, Salvador Eslava, Eleonora D'Elia, Robert Christopher Maher, Francisco Guitian, Eduardo Saiz

Angaben zur Veröffentlichung / Publication details:

García-Tuñon, Esther, Suelen Barg, Jaime Franco, Robert Bell, Salvador Eslava, Eleonora D'Elia, Robert Christopher Maher, Francisco Guitian, and Eduardo Saiz. 2015. "Printing in three dimensions with graphene." *Advanced Materials* 27 (10): 1688–93. https://doi.org/10.1002/adma.201405046.

Printing in Three Dimensions with Graphene

Esther García-Tuñon, Suelen Barg,* Jaime Franco, Robert Bell, Salvador Eslava, Eleonora D'Elia, Robert Christopher Maher, Francisco Guitian, and Eduardo Saiz*

Despite the significant progress achieved in the development of 2D printable electronics with graphene,[1–3] the additive manufacturing of 3D graphene structures remains a challenge. However, the payoff could be very big as graphene optical, electrical, mechanical, and thermal properties have the potential to open new engineering prospects well beyond electronics; from energy storage and transfer to sensing, catalysis, separation or structural, and functional composites.[3–7] A very apt technology for building macroscopic 3D graphene structures is robotic assisted deposition. This technique is based on the continuous extrusion of a suspension or ink with very specific rheological behavior. An effective way to achieve this behavior is to control accurately the interactions between graphene sheets in the suspension. In this respect, the use of chemically modified graphene (namely graphene oxide GO and its reduced form rGO) opens many possibilities. CMG sheets have tunable surface chemistry, interfacial activity, and solution processability making them a promising candidate for the integration of graphene into additive manufacturing.[1,8–10] Chemically modified graphene has been used in the wet processing of porous monoliths and even wires from oil/water emulsions.[9,11] However, to enable printing in three dimensions the filaments must have the right viscoelasticity to be able to maintain their shape after printing and to sustain the weight of a macroscopic printed part without deformation while exhibiting good adhesion to the previous layers. To address this challenge, in this work, we functionalize CMG with a responsive polymer (a branched copolymer surfactant, BCS) to create "responsive" sheets whose interactions in water can be regulated using an external stimulus, in this case pH.[12–16] Using this approach it is possible to formulate water-based inks with viscoelastic properties optimized to print self-supporting 3D structures through nozzles with diameters ranging from 500 down to 100 μm (**Figure 1**). Additional treatments can be used to manipulate the chemistry and microstructure of the printed parts opening new possibilities in a wide range of key technological areas from energy storage to thermal management, sensing or catalysis.[9,11,17]

Dr. E. García-Tuñon, Dr. S. Barg, Dr. S. Eslava,
E. D'Elia, Prof. E. Saiz
Centre for Advanced Structural Ceramics
Department of Materials
Imperial College London
London, SW7 2BP, UK
E-mail: egarciat@imperial.ac.uk;
suelen.barg@imperial.ac.uk
Dr. J. Franco
Keramat S. L.
Poligono Novo Milladoiro
A Coruña, Spain
R. Bell
Department of Chemistry
University of Warwick
Coventry, CV4 7AL, UK
Dr. S. Eslava
Department of Chemical Engineering
University of Bath
Bath, BA2 7AY, UK
Dr. R. C. Maher
The Blackett Laboratory
Imperial College London
London, SW7 2BZ, UK
Prof. F. Guitian
Instituto de Ceramica de Galicia
Universidad de Santiago de Compostela, Spain

GO is an atomically thin layer of carbon covalently bonded to different oxygen functional groups remaining from the chemical process used to exfoliate graphite.[1] Hydroxyl and epoxy groups are distributed within the basal plane along with un-oxidized graphitic islands, and carboxylic groups on the edges.[1] These carboxylic groups remain deprotonated at basic pH (Figure 1a).[18] BCS is a copolymer composed of two main domains: poly(methacrylic acid) (PMA) and polyethylene glycol (PEG), which are crosslinked with ethylene glycol dimethacrylate (EGDMA) to provide a branched architecture.[12,13,15,16] Each polymer chain end contains 1-dodecanethiol (DDT), which offers multiple hydrophobic anchoring groups (Supporting Information and Figure 1a). The composition and architecture of BCS provide multiple functional groups that enable the adsorption of BCS molecules on GO in a water suspension. Attractive interactions between the hydrophobic DDT anchoring groups in the BCS structure (Scheme S1 and S2, Figure S1, Supporting Information) and the hydrophobic graphitic islands of GO always take place, independently of pH range. In addition, there are adsorption mechanisms of BCS on GO that are pH-dependent as varying the pH modifies the ionization of GO[18] and BCS functionalities (Supporting Information, Scheme S3). These interactions enable the BCS-functionalization of GO sheets.

BCS provides electrostatic and steric stabilization of the GO suspension at basic pH (>6.46) through: i) electrostatic repulsions between the MA functional groups; and ii) steric repulsions between the EG functionalities in BCS molecules functionalizing the basal plane of the sheets and the GO ionized edges (Figure 1b). As a result it is possible to prepare stable suspensions with relatively high GO contents (up to 3 wt%/v%). The GO/BCS suspensions at basic pH show a shear thinning behavior as well as predominantly elastic response at strains below 10% (Figure S8, Supporting Information). Despite this viscoelastic behavior, the magnitude of the storage modulus is not high enough to hold the weight of free standing 3D objects printed by continuous extrusion. When the pH is decreased (below 6.46—pKa of BCS molecules) the carboxylic groups in the BCS and the GO edges start to protonate enabling the formation of multiple hydrogen bonds. At pH

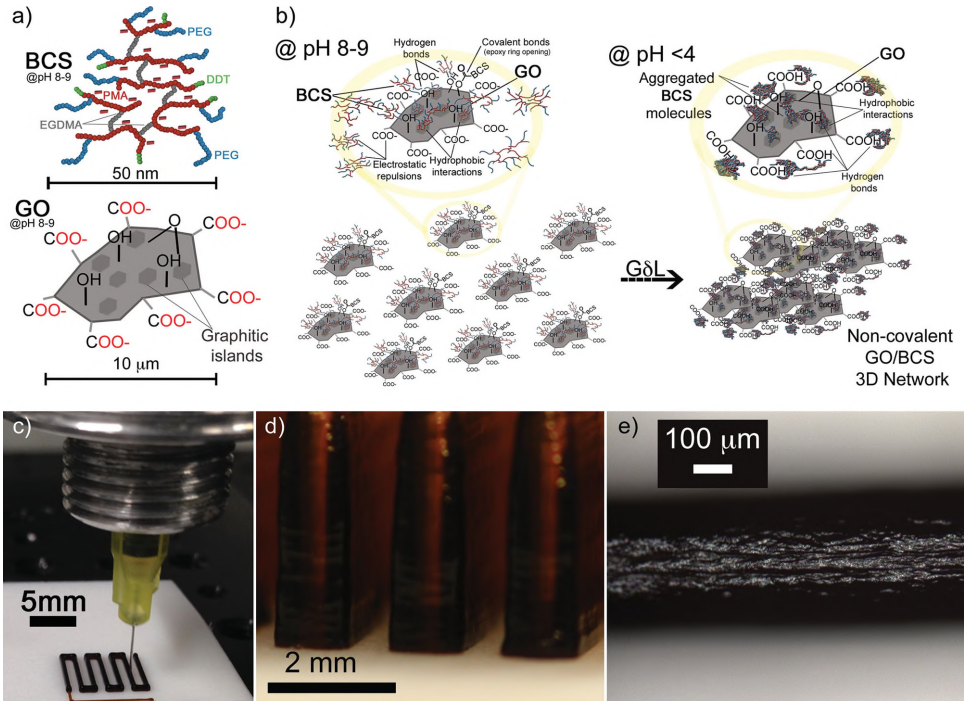

Figure 1. a) Simplified schematics depicting the proposed BCS and GO structures at basic pH (>6.46). Top: Composition and architecture of BCS: cross-linked PMA and PEG domains provide a branched structure with multiple hydrophobic anchoring groups DDT. Bottom: GO structure showing the distribution of functional groups on the basal plane (hydroxyl, epoxy, and unoxidized graphitic islands) and edges (carboxylic groups). b) Sketch of the directed assembly mechanism. BCS molecules attach to the basal plane of GO sheets at basic pH by: i) covalent bonding due to epoxy ring by nucleophilic attack, ii) hydrogen bonds between the GO hydroxyl groups and the EG groups in BCS, and iii) hydrophobic interactions between DDT anchoring groups and graphitic islands. When lowering the pH below ≈4, the protonation of COO^- groups in BCS branches and GO sheets leads to the establishment of multiple hydrogen-bonds and directs the assembly of GO sheets into a 3D network. c) Building a filament pile through a 100 μm nozzle with a low concentrated GO/BCS ink (1.75 wt%). d) Macroscopic image showing the fine details of piled up lines printed by continuous extrusion through a nozzle with a diameter of 100 μm. e) Optical microscopy of a filament immediately after printing through a 100 μm nozzle. Certain degree of filament expansion is observed. An increase of solid concentration of the ink helps preserving filament dimensions by increasing its "strength" (G')).

below 3.88, all the carboxylic groups are protonated; multiple non-covalent interactions between MA and EG functional groups can take place inside the BCS molecules and between molecules.[12,15] Non-covalent interactions can also take place between the MA and EG groups in BCS and the protonated carboxylic groups in GO edges. A gradual and homogeneous pH drop can be triggered by the addition of gluconic-δ-lactone (GδL) that dissolves and then hydrolyzes in water to gluconic acid.[13,14] The consequence is the formation of a GO/BCS 3D network linked by non-covalent interactions and an increase in the loss and storage modulus of more than 5 orders of magnitude (above 100 kPa, **Figure 2**b,c and Figure S8, Supporting Information). This network forms a water-based "pseudo-gel" with shear thinning behavior and a predominantly solid-like behavior at strains up to 1% (Figure S8, Supporting Information). Due to the non-covalent nature of the interactions the network-links can break down under shear (Figure S8, Supporting Information) enabling the easy flow of the gel through nozzles with diameters down to 100 μm (Figure 2d,e). Once the stress is released the links can heal. The GO/BCS network recovers its "pseudo-gel" structure and sets immediately after passing through the nozzle retaining the shape of the filament and holding the printed structure without deformation (Figure 1c–e). In this way it is possible to build 3D objects layer-by-layer using continuous extrusion (Figure 2d,e and Supporting Information, Movie S1).

Freestanding and stable GO 3D filament piles, rings, or woodpile structures with different shapes (**Figure 1**–**4**) were built in air through nozzles with internal diameters ranging from 100 to 500 μm using pressures between 1 and 4 bar depending on ink formulation. The printing speeds ranged between 4 and 10 mm s^{-1}. The inks contain from 1.75 wt% to 3 wt% GO and small amounts of additives (GO/BCS ratio of 6/1, GδL/BCS ratio around 3.8/1, and GO/organics (BCS and GδL) ratio of 1.3/1). The structures maintain their shape after printing and are strong enough to be handled. Subsequently, freeze drying is used to remove the water while preserving the 3D architecture and limiting shrinkage in order to maintain good dimensional control (Supporting Information).[19–21] The process leads to 3D objects with smooth surfaces and microscopic porosity while maintaining fine printing features down to the micrometer range (**Figure 3**).

After printing, thermal treatments (e.g., at temperatures ranging from 900 to 1000 °C in Ar/H_2 (10%) atmospheres) can be used to reduce GO while decomposing BCS and GδL.[22,23] Reduction is accompanied by 76% ± 1% weight loss for lower concentrated inks (ranging from 1.7 wt% to 2 wt% GO) and 81% ± 7% weight loss for the more concentrated

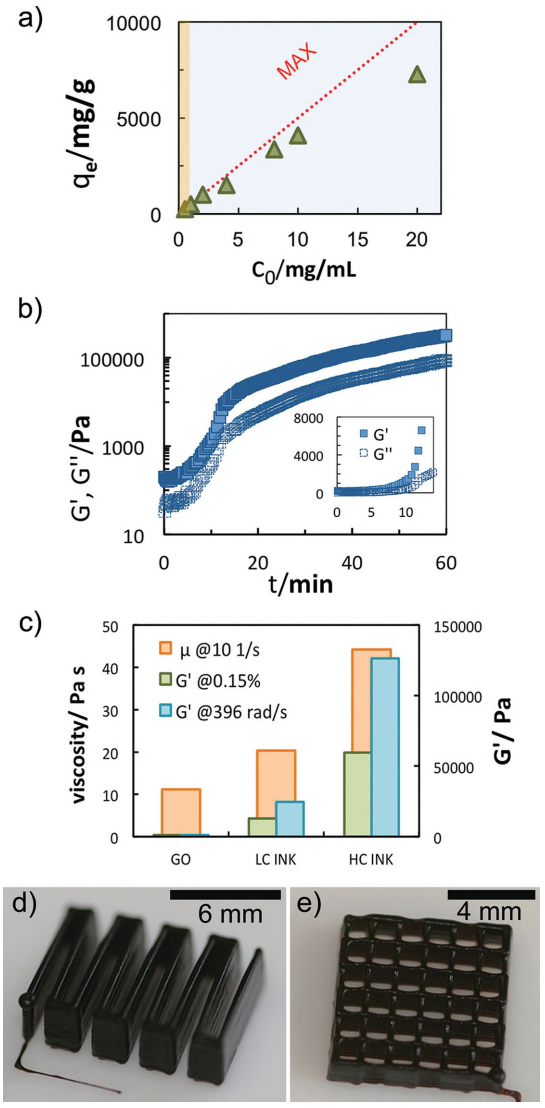

Figure 2. a) The degree of BCS adsorption on GO can be quantified by measuring the attachment of BCS modified with small amounts of rhodamine (BCSr) (Supporting Information) to GO surfaces. The graph shows the adsorption data plotted against the initial BCSr concentrations (C_0). BCSr interacts strongly with graphene oxide. At low initial BCSr concentrations (between 0.5 and 2 mg mL^{-1} at pH > 8, corresponding to GO/BCSr ratios between 4 and 1), all the BCSr molecules are adsorbed on the GO sheets. The dotted line indicates the limit at which all BCS molecules are absorbed on GO. The region highlighted in orange indicates the range of BCS concentrations used in GO/BCS inks for 3D printing. b) Kinetics of self-assembly followed with a time sweep at fixed strain (1%) and frequency (0.1 Hz). As time progresses GδL decomposes and the pH decreases. During assembly of the inks the pH typically varies between 8.5 and 10 (before) down to 3.2 and 4.3 (after adding the pH trigger) depending on ink formulation. The viscoelastic properties increase 5 orders of magnitude due to the formation of a 3D network of functionalized GO sheets. c) Histogram showing a comparison of the viscosity and storage modulus (*G'*) of a GO suspension (1.75 wt%) without additives (left), a GO/BCS suspension with low graphene oxide concentration (1.75 wt%, LC, middle), and a highly concentrated GO/BCS ink (2.5 wt% GO, HC, right). The viscosity at a shear rate of 10 s^{-1} increases from 10 to nearly 50 Pa s. d, e) 3D-printed graphene structures using robotic assisted deposition. Images showing filament pile and woodpile structures printed through a 150 μm nozzle with a highly concentrated GO/BCS ink (2.5 wt% GO).

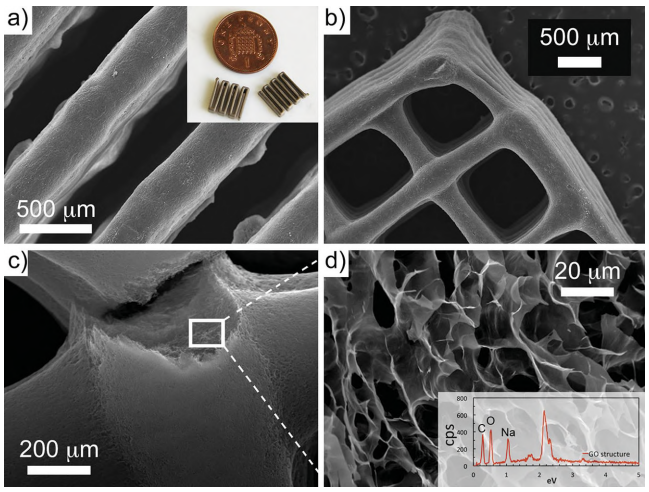

Figure 3. a) Piled up filaments and b) woodpile GO freeze-dried structures (printed through 500 and 150 μm nozzles respectively) after drying. The woodpile structure exhibits good bonding between layers and good definition. c,d) Fracture of a junction in a woodpile structure printed through 500 μm nozzle showing the inner microstructure of the printed lines. The lines have densities ranging from 25 to 65 mg cm^{-3} depending on ink formulation (before thermal reduction to rGO). The ice crystals formed during freeze-drying template the formation of a porous architecture inside the printed lines at the microscopic level resulting in highly porous structures with smooth surfaces. The inset in (d) shows an EDS analysis of the freeze-dried structure before reduction. Quantitative EDS analysis before reduction indicate that the dried structures are composed mainly by carbon, oxygen, and small amounts of Na (62% C, 35% O, and 3%Na). Peaks not labeled correspond to the conductive Au coating used for scanning electron microscopy. The sodium impurities come from the NaOH used to regulate the pH during the formulation of the inks.

ones (ranging between 2.5 wt% and 3 wt% GO). Because the amount of additives is very small[17,24] the degree of residual carbon left from additive decomposition will be very limited. After reduction, structures from higher-concentrated inks shrunk macroscopically over 4–7%. The measured shrinkage of the filament diameters ranges from 5% to 20% depending on the shape of the structure and the ink concentration. The resulting rGO objects are ultra-light and retain their shape, structural integrity, and inner microstructure (Figure 4). EDS shows a significant decrease in oxygen content upon reduction and Raman spectroscopy confirms the formation of predominantly crystalline rGO (Figure 4).[25] The electrical conductivity of the printed lines after reduction reaches values of 0.4 S cm^{-1} for filaments with densities around 6 mg cm^{-3}. These conductivities are comparable to those reported for other rGO porous networks (Figure S11, Supporting Information).[9,11,26,27]

All the structures have an elastomeric behavior and show between 96% and 90% recoverable deformation after 1–5 cycles of compression up to 20% strain (Figure 4), with stiffness and yield stress values in accordance to other porous graphene materials (Figure S11, Supporting Information).[9,11,28–30] Prior to reduction the GO sheets are linked together by the BCS molecules that contribute to the mechanical response (Figure 4g). The reduction treatment burns out the BCS, decreases the density of the structures, and breaks the non-covalent links in the

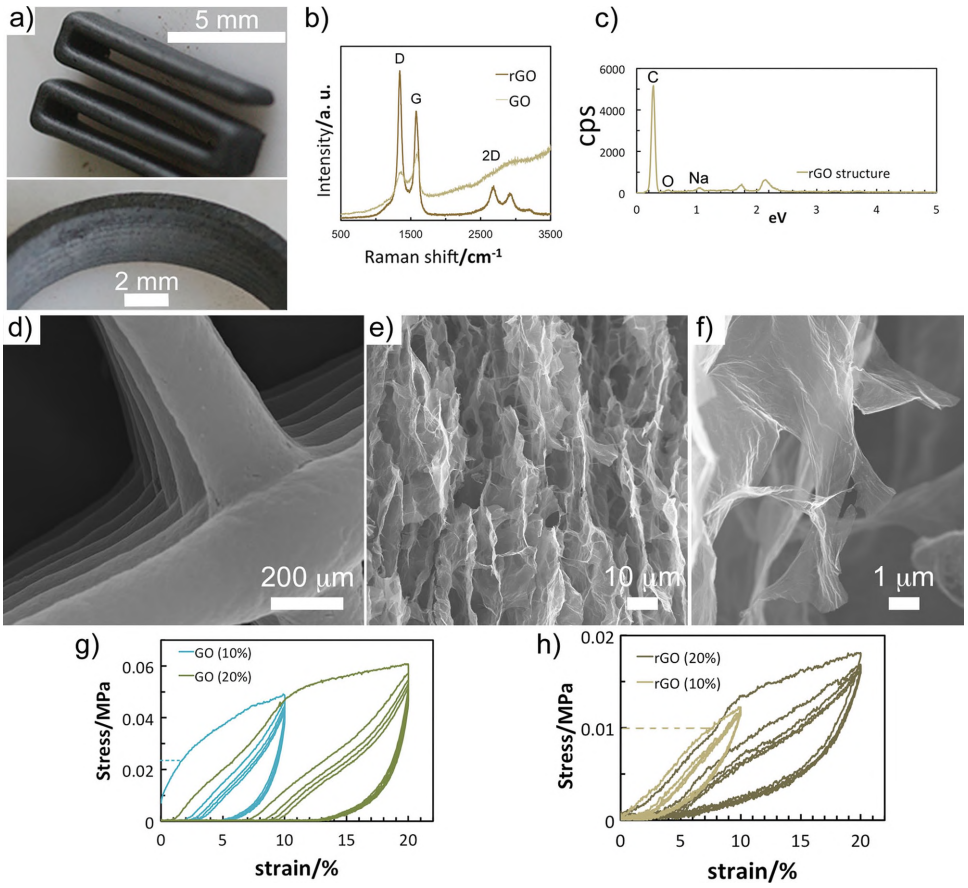

Figure 4. a) Images of rGO filament pile (top) and ring (bottom) structures printed through a 500 μm nozzle after thermal reduction. b) Raman spectra before and after reduction. The analysis after annealing confirms the recrystallization of graphene. The letters D, G, and 2D represent characteristic Raman active modes for graphene.[25] c) EDS analyses after thermal treatment confirm the reduction of GO with small amounts of remaining oxygen and Na impurities (92% C, 7% O, 1%Na). The final densities of the rGO objects range between 6 and 20 mg cm^{-3}. d) SEM image of the woodpile structure printed through a 150 μm nozzle (same as in Figures 2e and 3b)) after reduction. The image shows the microstructural detail of a junction between printed lines. There is good bonding and good layer definition in the 3D structure. The filaments retain their shape after reduction. e) The internal microstructure provided by the ice growth is preserved after the annealing treatment. f) High magnification image of a fracture surface showing the thin ice templated walls. g,h) Comparison of the mechanical properties of a 3D printed structure (piled up filament type, Figure S10c, Supporting Information) before ($\rho_{(GO\ structure)}$ = 17 mg cm^{-3}) (g) and after ($\rho_{(rGO\ structure)}$ = 6 mg cm^{-3})) (h) the reduction process. Nonreduced parts have higher yield stress (dashed lines in the graph, ≈0.025 MPa and 0.01 MPa for GO and rGO respectively) and Young modulus (E_{GO} = 0.84 MPa, E_{rGO} = 0.13 MPa) due to the presence of BCS linking the graphene sheets.

network (Figure 4h). As a consequence, nonreduced parts are stronger and stiffer than the reduced ones (Figure 4g,h). The estimated energy loss coefficients (energy dissipated in the material divided by the compression work in the first cycle) are of the order of 0.85 and 0.65 before and after thermal reduction respectively. These values are comparable to those measured for porous CMG monoliths.[9]

The ability to print 2D materials in three dimensions has huge potential to open up multiple possibilities in the design and "on demand" fabrication of new devices. We have shown how functionalization with BCS can be used to formulate CMG inks with the viscoelastic response needed to build practical 3D structures with precision and reliability using robotic assisted deposition. The inks allow printing through nozzles as thin as 100 μm and their rheology could also be tailored for other processing technologies such as extrusion, gel, or tape casting. Thermal annealing has been used to form electrically conductive rGO parts without compromising the structure and preserving the multifunctional properties of rGO. Alternatively, the mechanical stability of the printed parts may allow the use of additional treatments (e.g., chemical or electrochemical reduction) to further manipulate the properties without compromising the structure. By effectively extending the materials palette in AM technologies to include novel compounds, it will be possible to create new technological opportunities in the fabrication of devices and nanocomposites on demand for a wide range of applications in energy, environment, health, or transportation.

Experimental Section

BCS was synthesized following the protocol described by Woodward et al. (Supporting Information).[15] Rhodamine was incorporated into

the branched architecture in order to quantify BCS concentrations with UV–vis spectroscopy. Standard solutions of BCS-rhodamine (BCSr) with concentrations ranging from 0.001 wt/v% to 5 wt/v% were prepared in distilled water at pH 8 and measured in UV–vis spectrometer to obtain the calibration curve by plotting the absorbance versus concentration at 566 nm. Afterwards, the supernatants of GO/BCSr suspensions containing 0.2 wt% GO sheets and increasing amounts of BCSr (ranging from 0.001 wt/v% to 5 wt/v%) were analyzed by UV–vis spectroscopy after centrifugation. The BCS adsorption isotherm on GO sheets was determined by comparing the UV–vis absorbance at the excitation wavelength for rhodamine (566 nm).

GO solutions were prepared using a modified Hummers method (Supporting Information).[31] GO/BCS solutions were prepared by mixing different amounts of BCS stock solution (8 wt/v% in distilled water at pH 12) and GO suspension, keeping the GO/BCS ratio 6 to 1. Printable GO networks were prepared by lowering the pH of GO/BCS suspensions, with glucono-δ-lactone (GδL). The total content of organics was fixed at 1.3 (GO/organic content (BCS and GδL)).

The flow behavior and viscoelastic properties of GO suspensions (pH > 8) and inks (pH < 5) were measured in a Discovery Hybrid Rheometer HR1 (TA Instruments). The flow experiments were carried out with a parallel plate (ø = 40 mm) and a solvent trap cover under steady sensing. The self-assembly process was monitored by measuring the viscoelastic properties (G', G'') over time, immediately after lowering the pH of GO-BCS suspensions. The oscillation measurements (time sweeps with fixed frequency (0.1 Hz) and strain ($\gamma = 1\%$)) were applied immediately after adding the pH trigger. A solvent trap cover prevented water evaporation, while the axial force control allowed identifying changes in volume as well as automatically adjusting the gap. Viscoelastic fingerprints and linear viscosity region (LVR) were evaluated with stress-controlled amplitude sweeps at a fixed frequency of 396 rad s^{-1}, and stress-controlled frequency sweeps at a fixed strain of 0.15% (Supporting Information).

GO/BCS inks were used to print 3D objects using a robotic deposition device (Robocad 3.0, 3-D Inks, Stillwater, OK). The diameter of the printing nozzles ranged from 100 to 500 µm (EFD precision nozzles, EFD, East Providence, RI, USA). The inks were prepared at least 24 h before printing to ensure a stable rheological response. The pressure was regulated during printing in air to maintain constant ink flow.

3D printed GO structures were frozen in liquid nitrogen and subsequently freeze-dried (Freezone 4.5, Labconco Corporation). Once dried, samples were reduced in a tubular furnace (Carbolite Furnaces) at 950 °C in a 10%H_2/90%Ar atmosphere.

The microstructure and chemical composition were studied by field emission scanning electron microscopy on a LEO Gemini 1525 FEGSEM equipped with an energy dispersive spectroscopy (EDS) microprobe (INCA Sight Oxford-instruments, UK). All nonreduced samples and some of the reduced ones were coated with a thin gold layer previous to the observation. Raman spectroscopy was performed using a Renishaw RM2000 equipped with a 514 nm laser.

The mechanical tests were carried out in a Zwick universal testing machine with a maximum load of 2 kN. The 3D structures were subjected to cyclic compression in the direction perpendicular to the printing plane: up to 5 cycles at 10% and 20% strain, with a holding period of 30 s under position-controlled movement of 1 mm min^{-1}.

A standard 4-point probe method was used for conductivity measurements. The current was generated via a bench top PSU and kept at a constant direct current of 10 mA. Two electrodes were placed through the sample at constant distance to monitor the voltage drop through the sample. The results were derived via standard equations for electrical conductivity and resistivity in DC.

Supporting Information

Supporting Information is available from the Wiley Online Library or from the author.

Acknowledgements

The authors would like to acknowledge the EPSRC grant Graphene 3D Networks (EP/K01658X/1). S.B. would like to acknowledge the European Commission (FP7 Marie Curie Intra-European Fellowship ACIN). S.E. would like to acknowledge EPSRC grant Engineering with Graphene for Multifunctional Coatings and Fiber-Composites EP/K016792/1. E.S. and E.G.T. would like to acknowledge the support of RFEC-ATL, ONRG, and DARPA.

[1] F. Kim, L. J. Cote, J. Huang, *Adv. Mater.* **2010**, *22*, 1954.
[2] S. Wang, P. K. Ang, Z. Wang, A. L. L. Tang, J. T. L. Thong, K. P. Loh, *Nano Lett.* **2010**, *10*, 92.
[3] F. Torrisi, T. Hasan, W. Wu, Z. Sun, A. Lombardo, T. S. Kulmala, G.-W. Hsieh, S. Jung, F. Bonaccorso, P. J. Paul, D. Chu, A. C. Ferrari, *ACS Nano* **2012**, *6*, 2992.
[4] A. K. Geim, K. S. Novoselov, *Nat Mater* **2007**, *6*, 183.
[5] G. Eda, G. Fanchini, M. Chhowalla, *Nat. Nanotechnol.* **2008**, *3*, 270.
[6] S. Stankovich, D. A. Dikin, G. H. B. Dommett, K. M. Kohlhaas, E. J. Zimney, E. A. Stach, R. D. Piner, S. T. Nguyen, R. S. Ruoff, *Nature* **2006**, *442*, 282.
[7] M. D. Stoller, S. Park, Y. Zhu, J. An, R. S. Ruoff, *Nano Lett.* **2008**, *8*, 3498.
[8] C. Cheng, D. Li, *Adv. Mater.* **2012**, *25*, 13.
[9] S. Barg, F. M. Perez, N. Ni, P. do V Pereira, R. Maher, E. Garcia-Tunon, S. Eslava, S. Agnoli, C. Mattevi, E. Saiz, *Nat. Commun.* **2014**, *5*, 1.
[10] S. Naficy, R. Jalili, S. H. Aboutalebi, R. A. Gorkin III, K. Konstantinov, P. C. Innis, G. M. Spinks, P. Poulin, G. G. Wallace, *Mater. Horiz.* **2014**, *1*, 326.
[11] L. Qiu, J. Z. Liu, S. L. Y. Chang, Y. Wu, D. Li, *Nat. Commun.* **2012**, *3*, 1241.
[12] J. V. M. Weaver, S. P. Rannard, A. I. Cooper, *Angew. Chem.* **2009**, *121*, 2165.
[13] D. E. García-Tuñon, S. Barg, R. Bell, J. V. M. Weaver, C. Walter, L. Goyos, E. Saiz, *Angew. Chem. Int. Ed.* **2013**, *52*, 7805.
[14] R. T. Woodward, L. Chen, D. J. Adams, J. V. M. Weaver, *J. Mater. Chem.* **2010**, *20*, 5228.
[15] R. T. Woodward, C. Hight, U. Yildiz, N. Schaeffer, E. M. Valliant, J. R. Jones, M. M. Stevens, J. V. M. Weaver, *Soft Matter* **2011**, *7*, 7560.
[16] R. T. Woodward, J. V. M. Weaver, *Polym. Chem.* **2011**, *2*, 403.
[17] L. Zhang, F. Zhang, X. Yang, G. Long, Y. Wu, T. Zhang, K. Leng, Y. Huang, Y. Ma, A. Yu, Y. Chen, *Sci. Rep.* **2013**, *3*, 1408.
[18] B. Konkena, S. Vasudevan, *J. Phys. Chem. Lett.* **2012**, *3*, 867.
[19] J. A. Lewis, *J. Am. Ceram. Soc.* **2000**, *83*, 2341.
[20] J. E. Smay, J. Cesarano, J. A. Lewis, *Langmuir* **2002**, *18*, 5429.
[21] J. J. Guo, J. A. Lewis, *J. Am. Ceram. Soc.* **1999**, *82*, 2345.
[22] A. Bagri, C. Mattevi, M. Acik, Y. J. Chabal, M. Chhowalla, V. B. Shenoy, *Nat. Chem.* **2010**, *2*, 581.
[23] S. Pei, H.-M. Cheng, *Carbon* **2012**, *50*, 3210.
[24] V. Dua, S. P. Surwade, S. Ammu, S. R. Agnihotra, S. Jain, K. E. Roberts, S. Park, R. S. Ruoff, S. K. Manohar, *Angew. Chem. Int. Ed.* **2010**, *49*, 2154.
[25] L. G. Cançado, A. Jorio, E. H. M. Ferreira, F. Stavale, C. A. Achete, R. B. Capaz, M. V. O. Moutinho, A. Lombardo, T. Kulmala, A. C. Ferrari, *Nano Lett.* **2011**, 3190.

[26] X. Zhang, Z. Sui, B. Xu, S. Yue, Y. Luo, W. Zhan, B. Liu, *J. Mater. Chem.* **2011**, *21*, 6494.
[27] Z. Chen, W. Ren, L. Gao, B. Liu, S. Pei, H.-M. Cheng, *Nat. Mater.* **2011**, *10*, 424.
[28] M. A. Worsley, S. O. Kucheyev, J. H. Satcher Jr., *Appl. Phys. Lett.* **2009**.
[29] X. Xie, Y. Zhou, H. Bi, K. Yin, S. Wan, L. Sun, *Sci. Rep.* **2013**, *3*, DOI 10.1038/srep02117.
[30] H. Hu, Z. Zhao, W. Wan, Y. Gogotsi, J. Qiu, *Adv. Mater.* **2013**, *25*, 2219.
[31] M. Hirata, T. Gotou, S. Horiuchi, M. Fujiwara, M. Ohba, *Carbon* **2004**, *42*, 2929.